6188 J. Med. Chem. 2010, 53, 6188–6197
DOI: 10.1021/jm1005868

Journal of Medicinal Chemistry Article

Novel Octreotide Dicarba-analogues with High Affinity and Different Selectivity for Somatostatin Receptors

Alessandra Di Cianni,[†,‡] Alfonso Carotenuto,[*,§] Diego Brancaccio,[§] Ettore Novellino,[§] Jean Claude Reubi,[∥] Karin Beetschen,[∥] Anna Maria Papini,[†,‡] and Mauro Ginanneschi[*,†,‡]

[†]*Laboratory of Peptides & Proteins, Chemistry & Biology, University of Firenze, Via della Lastruccia 13, I-50019 Sesto Fiorentino, Italy,* [‡]*Department of Chemistry "Ugo Schiff", University of Firenze, Via della Lastruccia 5-13, I-50019, Sesto Fiorentino, Italy,* [§]*Department of Pharmaceutical Chemistry and Toxicology, University of Napoli, Via Domenico Montesano 49, I-80131 Napoli, Italy, and* [∥]*Division of Cell Biology and Experimental Cancer Research, Institute of Pathology, University of Berne, Murtenstrasse 31, CH-3010 Berne, Switzerland*

Received May 17, 2010

A limited set of novel octreotide dicarba-analogues with non-native aromatic side chains in positions 7 and/or 10 were synthesized. Their affinity toward the $ssts_{1-5}$ was determined. Derivative **4** exhibited a pan-somatostatin activity, except sst_4, and derivative **8** exhibited high affinity and selectivity toward sst_5. Actually, compound **8** has similar sst_5 affinity (IC_{50} 4.9 nM) to SRIF-28 and octreotide. Structure−activity relationships suggest that the *Z* geometry of the double-bond bridge is that preferred by the receptors. The NMR study on the conformations of these compounds in SDS_{-d25} micelles solution shows that all these analogues have the pharmacophore β-turn spanning Xaa[7]-D-Trp[8]-Lys[9]-Yaa[10] residues. Notably, the correlation between conformation families and affinity data strongly indicates that the sst_5 selectivity is favored by a helical conformation involving the C-terminus triad, while a pan-SRIF mimic activity is based mainly on a conformational equilibrium between extended and folded conformational states.

Introduction

The cyclic tetradecapeptide somatostatin (H-Ala[1]-Gly[2]-*c*[Cys[3]-Lys[4]-Asn[5]-Phe[6]-Phe[7]-Trp[8]-Lys[9]-Thr[10]-Phe[11]-Thr[12]-Ser[13]-Cys[14]]-OH, SRIF-14[a]) was first isolated from mammalian hypothalamus.[1] This hormone is widely distributed in the human body and is found in the gut, pancreas, nervous system, and in some exocrine and endocrine glands. By interactions with a family of five SRIF receptors (ssts), the native peptide exerts a great number of regulatory effects, especially those related to GH release. Different receptor subtypes mediate various functions, but only sst_2 and sst_5 activities have been precisely related to specific physiological activities.[2] SRIF receptors are strongly expressed in various types of malignant cells, particularly in some neuroendocrine or neuroendocrine-like tumors. Over the last three decades, this has prompted researchers to prepare a huge number of new cyclic and acyclic analogues, which are more stable than SRIF in physiological conditions. Among these, a large number of reduced-size cyclic analogues, with or without the disulfide bridge, were synthesized and tested for their affinity toward the ssts. Furthermore, their pharmacological behavior was studied and several NMR investigations on their affinity/conformations relationships were carried out. J. E. Rivier's group, at the Salk Institute of La Jolla, carried out a careful structure/affinity study on SRIF analogues, introducing non-natural amino acids in the sequence and preparing variably sized S−S bridged cyclopeptides. These authors related the structure/conformation of the cyclopeptides to the sst_{1-4} specific affinity by means of NMR studies.[3−6]

Octreotide[7] (compound **1**, Figure 1), a cyclic octapeptide analogue of somatostatin, containing a disulfide tether and showing high affinity and selectivity for sst_2, was the first analogue to be used in clinical protocols. Following the enormous growth in preparation and application of radiolabeled peptides for tumor imaging and therapy, the somatostatin analogues thus far obtained were designed mainly for the targeting of malignant cells with γ- or β-emitting radionuclides.[4,8,9] As a matter of fact, octreotide derivatives [^{111}In-DTPA]octreotide (OctreoScan) and [^{90}Y-DOTA-Tyr[3]]octreotide (OctreoTher) are both quite successfully used in the clinical diagnosis and therapy of neuroendocrine tumors, respectively.[10] Nevertheless, the vulnerability of the S−S bridge to endogenous and

*To whom correspondence should be addressed. For A.C.: phone, +39-081-678626; fax, +39-081-678644; E-mail, alfonso.carotenuto@unina.it. For M.G.: phone, +39-055-4573525; fax, +39-055-4573531; E-mail: mauro.ginanneschi@unifi.it.

[a] Abbreviations Bzl, benzyl; dh-DSA-C, dehydrodiaminosuberic acid, C-terminus; dh-DSA-N, dehydrodiaminosuberic acid, N-terminus; DMF, dimethyl formamide; DMSO-d_6, hexadeuteriodimethylsulfoxide; DOTA, 1,4,7,10-tetraazacyclododecane-1,4,7,10-tetraacetic acid; DQF-COSY, double quantum filtered-correlation spectroscopy; EDT, 1,2-ethanedithiol; ESI-MS, electrospray ionization-mass spectrometry; Fmoc, 9-fluorenylmethoxycarbonyl; GH, growth hormone; Hag, L-2-allyl-Gly; GPCR, G-protein coupled receptor; HATU, exafluorophosphate salt of the *O*-(7-azabenzotriazol-yl)-tetramethyl uranium cation (this acronym does not longer correspond to the true structure); LC, liquid chromatography; MD, molecular dynamics; MW, molecular weight; 1-Nal, 1-naphthyl-alanine; NMM, *N*-methyl morpholine; NOE, nuclear Overhauser effect; NOESY, nuclear Overhauser enhanced spectroscopy; RCM, ring closing metathesis; rmsd, root-mean-square deviation; RP-HPLC, reverse phase-high performance liquid chromatography; SDS, sodium dodecyl sulfate; SPE, solid phase extraction; SPPS, solid phase peptide synthesis; SRIF, somatostatin; sst, somatostatin receptor; TFA, trifluoroacetic acid; TOCSY, total correlated spectroscopy; TSP, [(2,2,3,3-tetradeuterio-3-(trimethylsilanyl)]propionic acid.

 Published on Web 07/28/2010

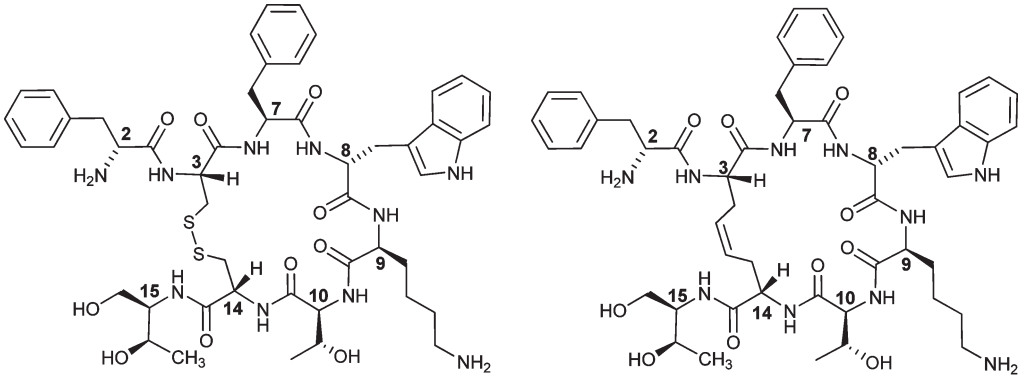

Figure 1. Structure of octreotide (SMS201-995) (**1**) and of the first dicarba SRIF mimetic (**2**).[12] (Note: numbering of the residues follows that of the native SRIF).

Table 1. Peptide Sequences: General Formula: D-Phe^2-*c*[dhDSA-N^3-Xaa^7-D-Trp^8-Lys^9-Yaa^{10}-dhDSA-C^{14}]-Thr(ol)^{15}-OH

peptide	*Xaa*^{7}	*Yaa*^{10}	double-bond geometry
2[a]	Phe	Thr	*Z*
3[a]	Phe	Tyr(Bzl)	*E*
4	Phe	Tyr(Bzl)	*Z*
5	1-Nal	Thr	*Z*
6	Phe	Tyr	*E*
7	Phe	Tyr	*Z*
8	1-Nal	Tyr(Bzl)	*Z*

[a] These compounds were previously reported.[13]

exogenous oxidating and reducing agents, such as those employed in the experimental conditions of labeling with the radioisotopes $^{99\,m}$Tc or ^{188}Re,[11] prompted us to synthesize dicarba-analogues of similar ring size by the RCM reaction on two allylglycines, substituting the relevant Cys^{3,14} residues in the linear peptide. Compound **2**, reported in Figure 1 as an example, is the first octreotide dicarba-tethered analogue synthesized by us and has the same amino acid sequence of the corresponding, S−S bridged, molecule.[12,13]

The resulting unsaturated dicarba bridge proved to be insensitive to the conditions used for $^{99\,m}$Tc or ^{188}Re labeling (unpublished results), and the molecules obtained were very stable in human serum.[12,13] Recently, the stability of these compounds was exploited in the successful conjugation of cytotoxic dichloroplatinum complexes to analogue **2** as well as to the double-bond hydrogenated derivative.[14] The same reaction, attempted with the octreotide molecule, failed. When the affinities of these analogues toward the five ssts were determined, we ascertained that some of them showed unexpected specific affinity for the sst$_5$ subtype, which led us to define a novel pharmacophore model for this receptor.[13]

This paper reports the synthesis of new cyclooctapeptide dicarba-analogues that have structures similar to those depicted in Figure 1 but are designed to carry different aromatic residues in positions 7 and/or 10 (Table 1). In the following, ssts subtypes affinities found for the new compounds **4**−**8** are correlated with the C=C bridge geometry and with the conformational behavior in SDS$_{-d25}$ micelles solution, investigated by NMR experiments. Characteristic structure−affinity relationships of this class of somatostatin analogues are widely discussed.

Results

Peptide Synthesis and Purification. The synthesis of dicarba-analogues followed the procedure described in our previous articles.[12,13] Starting from H-L-Thr(*t*Bu)-ol-2-chlorotrityl resin (0.5 mmol/g) already containing [Thr(ol)^{15}], the elongation of the peptide sequence was stopped after the coupling of Hag^3 residue, with the aim of removing any possible interference of the aromatic ring of D-Phe in the correct orientation of the allylglycine side chains. After the Fmoc−Hag^3 coupling, the resin loading (0.5 mmol/g) already met the requirements of the pseudodilution effect, minimizing the risk of the formation of intermolecular bonds. The linear heptapeptides were then converted by RCM by the second generation Grubbs catalyst (**9**) (Figure 2) to the corresponding cyclic analogues.

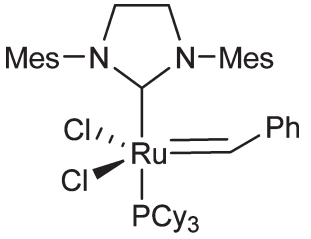

9

Figure 2. Second generation Grubbs catalyst.

The D-Phe^2 terminal residue was added only after ring-closing, thus facilitating the cyclization step. Cleavage of the crude peptides from the resin was obtained using the standard cleavage mixture TFA/H_2O/EDT/phenol (94:2:2:2, 3 h) for compounds **5**, **6**, and **7** and with the new percentage mixture (70:26:2:2, 2,30 h) for compounds **4** and **8** in order to overcome the loss of the benzyl group of the Tyr(Bzl) residue by hydrolysis, as described in our previous article.[13] All compounds obtained by RCM with **9** were prepurified by SPE. The concentrated compound adsorbed on the SPE was eluted with an increased percentage of CH_3CN in H_2O (from 0% to 100%). The fractions enriched with each desired compound were then purified by semipreparative RP-HPLC and characterized by ESI-MS. For each peptide, with the exception of **5** and **8**, the HPLC chromatogram showed two peaks with the same MW, corresponding to the geometric isomers (*Z*/*E* ratio ≈ 90:10). In particular, the *E* structure of the C−C=C−C tether of the sample eluted at lower R_t and the *Z* structure one of the second, more intense peak, was ascertained by ^{1}H NMR inspection. The HPLC purity of each compound studied was >97%, and the isolated compounds showed unique *E* or *Z* configuration, confirmed by NMR analysis. No oligomer byproduct were observed.

Table 2. Receptor Affinities of the Somatostatin Analogues

	IC_{50} (nM)[a]				
no.	sst_1	sst_2	sst_3	sst_4	sst_5
SRIF-28	2.3 ± 0.4 (7)	3.0 ± 0.2 (7)	3.6 ± 0.5 (7)	1.6 ± 0.3 (7)	2.4 ± 0.2 (6)
2[b]	>1000 (2)	44 ± 1 (2)	>1000 (2)	412 ± 68 (2)	28 ± 2 (2)
3[b]	>1000 (2)	> 1000 (2)	892 ± 245 (2)	>1000 (2)	29 ± 1 (2)
4	25 ± 1 (3)	46 ± 3 (3)	25 ± 4 (3)	346 ± 23 (3)	12.3 ± 0.3 (3)
5	>1000 (3)	9.6 ± 0.9 (3)	>1000 (3)	249 ± 51 (3)	16.5 ± 4.5 (3)
6	1000 (3)	355.5 ± 45.5 (3)	1000 (3)	1000 (3)	418 ± 56 (3)
7	>1000 (3)	87 ± 18 (3)	>1000 (3)	>1000 (3)	161 ± 27 (3)
8	57.5 ± 12.5 (3)	101 ± 9 (3)	92.5 ± 0.5 (3)	>1000 (3)	4.9 ± 1.0 (4)

[a] The number of independent repetitions to obtain the mean values ± SEM are indicated between brackets. SRIF-28 is used as internal control. [b] Corresponds to data published previously.[13]

Binding Affinity to sst_{1-5} Receptors. All compounds were tested for their ability to bind to the five human sst_{1-5} receptors subtypes in complete displacement experiments using the universal somatostatin radioligand [^{125}I]-[Leu^8, D-Trp^{22},Tyr^{25}]-somatostatin-28. SRIF-28 was run in parallel as control. IC_{50} values were calculated after quantification of the data using a computer-assisted image processing system. Binding data indicate that all compounds show sub-μM binding affinities toward the sst_5 (Table 2). Compounds **2** and **3** have already been described[13] and are reported for comparison. While peptide **3** was a potent and selective sst_5 ligand, its *Z*-isomer, peptide **4**, exhibited a pan-somatostatin affinity, apart from sst_4. In fact, the analogue **4** doubled the affinity toward sst_5 but completely lost the selectivity of **3**.

Peptide **5** is the 1-Nal^7 analogue of **2** (Table 1). This peptide exhibited a low nanomolar $sst_{2,5}$ affinity. Actually, it is the most potent sst_2 ligand among the dicarba-analogues prepared to date. The double-bond isomer analogues **6** (*E*) and **7** (*Z*), in which the phenolic group of Tyr^{10} replaces the Tyr(Bzl) residue of **3** and **4**, respectively, did not show any significant affinity toward sst_{1-5} subtypes apart from a slight affinity of **7** to sst_2.

Finally, analogue **8** shared Tyr(Bzl)^{10} residue with peptide **4** and 1-Nal^7 residue with peptide **5**. Like compound **4**, it showed affinity for all the receptor subtypes except sst_4. However, the significant enhancement of the sst_5 affinity (nearly 3-fold compared to compound **4**) and the simultaneous reduction of affinity toward sst_{1-4} make compound **8** a strong and selective sst_5 ligand. Indeed, compound **8** is the most potent sst_5 dicarba-analogue synthesized so far, showing an affinity close to the value found for the reference compound SRIF-28 (Table 2).

NMR Analysis. NMR analysis of the analogues **3**−**8** was performed by means of 1D and 2D proton homonuclear experiments. NMR experiments were recorded on a Varian Inova-Unity 700 MHz spectrometer. Spectra were collected in SDS_{-d25} (200 mM) micelles solution. All samples (about 2 mM) were kept at 308 K and at pH ≅ 5. Complete ^{1}H NMR chemical shift assignments were effectively achieved for all the analyzed molecules according to the Wüthrich procedure[15] via the usual systematic application of TOCSY[16] and NOESY[17] experiments with the support of the XEASY software package (Tables S3−S8, Supporting Information).[18] NMR-derived constraints obtained for all compounds, were used as the input data for a simulated annealing structure calculation, as implemented within the standard protocol of the DYANA program.[19]

Compound 3. The analogue **3** bears Tyr(Bzl) in position 10. We have already analyzed this peptide in our previous work in water/DMSO-d_6 solution.[13] The geometry of the double bond was confirmed as *trans* (*E*) from the coupling constant ($^3J_{CH=CH}$ = 15.1 Hz) between the two olefinic protons of the bridge and NOE contacts between the same olefinic and the H_βs of residue 14 (**3**). A qualitative analysis of short- and medium-range NOEs, $^3J_{NH\text{-}H\alpha}$ coupling constants, and temperature coefficients for exchanging NH was used to characterize the secondary structure of **3**. Spectra analysis pointed to the presence of a β-turn about residues 7−10. Interestingly, the upfield shift observed for H_γs of Lys^9 (δ = 0.52, 0.43 ppm) has been used for decades as diagnostic for biological activity.[20] NOE-derived constraints obtained for **3** were used as the input data for a simulated annealing structure calculation (Table S9, Supporting Information). The backbone arrangement of **3** was well-defined, possessing an average root-mean-square deviation (rmsd) of the heavy atoms equal to 0.15 Å. No violation higher than 0.1 Å was observed again, indicating conformational stability (Table S7, Supporting Information). Main backbone features were a type II′ β-turn spanning residues D-Trp^8-Lys^9, followed by a short 3_{10}-helix along residues Tyr(Bzl)^{10}-dhDsa-C^{14}-Thr-(ol)^{15} (Figure 3). The turn structure is stabilized by hydrogen bonds between Phe^7-CO and Tyr(Bzl)^{10}-NH. The helical structure is stabilized by H-bonds between D-Trp^8-CO and dhDsa-C^{14}-NH and between Lys^9-CO and Thr(ol)^{15}-NH. These bonds are typical of 3_{10}-helix structure (i, i + 3). The side chains of dhDsa-N^3, D-Trp^8, Lys^9, Tyr(Bzl)^{10}, and dhDsa-C^{14} showed well-defined χ1 values (i.e., *trans*, *trans*, *gauche*$^-$, *gauche*$^-$, and *gauche*$^+$ orientations, respectively). These orientations allowed a close spatial proximity between D-Trp^8/Lys^9 side chains; moreover, the tyrosyl group of the residue 10 points toward the Lys^9 side chain. In contrast, D-Phe^2 and Phe^7 side chain showed almost free rotation about the χ1 torsion angle. Also, the Bzl group of residue 10 was highly flexible.

Compound 4. The analogue **4** is the geometric (*Z*) isomer of **3** as established by the coupling constant ($^3J_{CH=CH}$ = 8.1 Hz) between the two olefinic protons of the bridge and the relative strong NOE between the same olefinic H_γs. This analogue shows spectral features similar to those found in **3** but with a greater tendency to conformational heterogeneity. In fact, NOESY spectra of **4** showed, simultaneously, both diagnostic connectivities consistent with folded structures $d_{\alpha N}(i, i + 2)$ between H_α-8/NH-10, H_α-9/NH-14, H_α-10/NH-15, and $d_{\alpha N}(i, i + 3)$ between H_α-9/NH-15 and NOE contacts characteristic of extended regions strong $d_{\alpha N}(i, i + 1)$ between H_α-9/NH-10, H_α-10/NH-14, and H_α-14/NH-15 (Table S10, Supporting Information). The apparently contradictory NOEs are indicative of the presence of at least two conformations in solution. The impossibility of resuming all the data in a single structure prompted us to consider incompatible NOEs separately in different calculation cycles

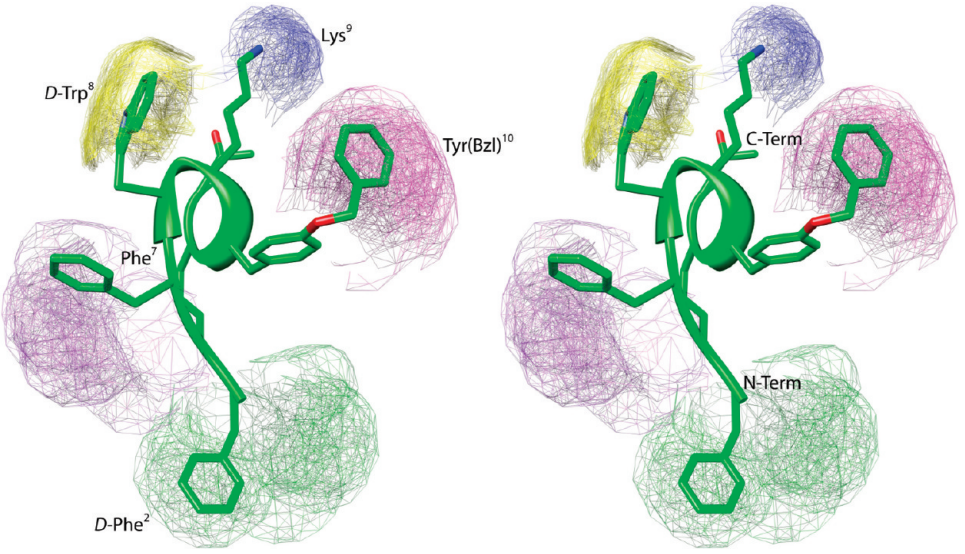

Figure 3. Stereoview of the lowest energy conformer of compound **3**. Backbone is evidenced as a ribbon. Side chains of the 10 lowest energy conformers are also shown as mesh surface. Surfaces are distinguished with different colors. N-Term, N-terminus; C-Term, C-terminus.

(Experimental Section). Hence, we obtained two families of conformations. The first calculation cycle gave an ensemble of structures (family I) showing a similar conformation to compound **3**, with a type II′ β-turn spanning residues D-Trp^8-Lys^9, followed by a short 3_{10}-helix along residues Tyr(Bzl)^{10}-dhDsa-C^{14}-Thr(ol)^{15} (Figure 4a). Moreover, side chain orientations were the same as those described for **3**. The main difference was a better definition of the Phe^7 side chain which preferred the *trans* rotamer. For this set of structures, a number of consistent violations were observed (Table S10, Supporting Information). In a second MD cycle, the violated upper limit constraints were upweighted for the contribution to the target function. Thus, a second conformational family (family II) was obtained which differed from the first mainly in that C-terminal residues were in extended conformations (Figure 4b). Furthermore, the side chain orientation of Tyr-(Bzl)^{10} was *trans*. Hence, the tyrosyl nucleus was further from the Lys^9 side chain. This is in accordance with the downfield shifts of the H_γ resonances of Lys^9 compared to the corresponding shifts of compound **3**. Interestingly, the complete ensemble of structures (helix and extended) fulfilled the NOE restraints, with no violations exceeding 0.5 Å (Table S10, Supporting Information).

Compound 5. Compound **5** maintains the same octreotide scaffold except for position 7, which bears 1-Nal. Apart from the dicarba bridge, it has the same peptide sequence of the analogue NOC, formerly prepared and studied as DOTA-conjugate by Maecke, Reubi, and co-workers.[21] The coupling constant ($^3J_{CH=CH}$ = 8.1 Hz) between the two olefinic protons of the bridge and the relative strong NOE between the same olefinic H_γs established (*Z*) configuration for compound **5**. Only one isomer is obtained from RCM.

NMR-based structure calculations gave two conformational families, like compound **4**. Family I, obtained by a first run of MD calculation, showed a type II′ β-turn spanning residues D-Trp^8-Lys^9, followed by a short 3_{10}-helix along residues Thr^{10}-dhDsa-C^{14}-Thr(ol)^{15} (Figure 5a). As found with compound **4**, a number of consistent violations were observed (Table S11, Supporting Information). In a second MD run, we obtained a second conformational family (II), which differed from the first mainly because the C-terminal residues were in extended conformations (Figure 5b). In both the families, residue 7 showed a defined *trans* orientation which forces 1-Nal^7 naphthyl moiety close to D-Trp^8 residue. This orientation is in accordance with the intense upfield shift observed for many D-Trp^8 proton resonances.

Compounds 6 and 7. The analogues **6** and **7** differ from compounds **3** and **4** in that the Tyr(Bzl)^{10} residue was replaced by a Tyr (i.e., without the Bzl group). Following the same arguments given for **3** and **4**, an *E* configuration was assigned to compound **6** and a *Z* configuration to the compound **7** at the double bond.

Many potential diagnostic NOEs could not be observed in the NOESY spectra of these analogues due to signal overlapping and this precluded structure calculations. For instance, H_α protons of Lys^9 and Thr-ol^{15} resonated at the same chemical shift for both peptides. Actually, the NMR parameters of **6** (H_α shifts, coupling constants, and temperature coefficients) are very similar to those of compound **3**, and this was also true for **4** and **7**. Therefore, it could be hypothesized that 3D structures should be similar too.

Compound 8. The analogue **8** structure was rationalized starting from the peptide sequence of the previous compounds **4** and **5**. In fact, it bears both 1-Nal^7 and Tyr(Bzl)^{10}. For compound **8**, a *Z* configuration was established from the NOEs and coupling constant ($^3J_{CH=CH}$ = 8.1 Hz) between the two olefinic protons. NMR-based structure calculation (Table S12, Supporting Information) gave two conformational families, as it did for compounds **4** and **5**, the first (family I) showing a short 3_{10}-helix along the Thr^{10}-dhDsa-C^{14}-Thr(ol)^{15} residues (Figure 6a), and the second (family II) an extended conformation along the same residues (Figure 6b). In both families, the D-Trp^8, Lys^9, and Tyr(Bzl)^{10} side chains were spatially closed in accordance with the increased upfield shift of the H_γ and H_β resonances of Lys^9. Differently from compound 5, 1-Nal^7 residue could not adopt a *trans* conformation, probably due to steric hindrance with Tyr(Bzl)^{10}. In fact, 1-Nal^7 side chain was preferentially in a *gauche*$^-$ conformation.

Discussion

In our ongoing efforts to develop new somatostatin ligands with improved stability and affinity toward sst receptors, we

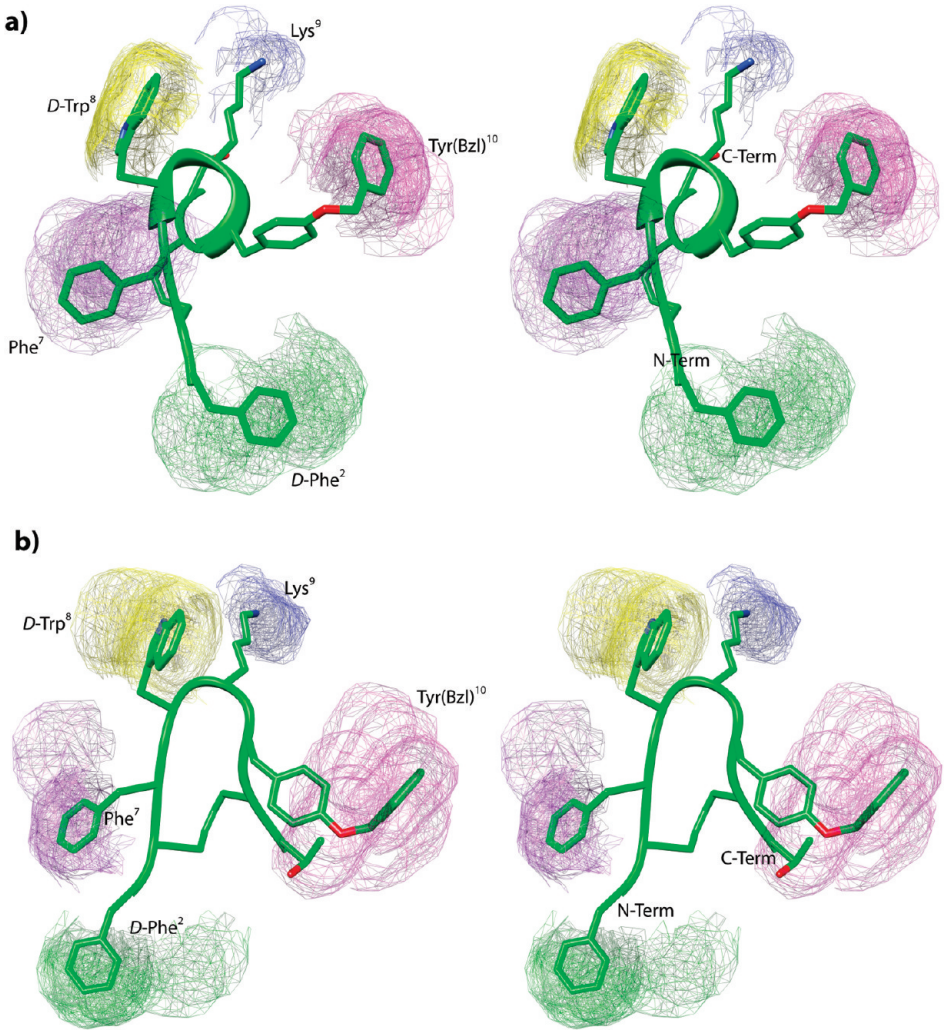

Figure 4. Stereoview of the lowest energy conformer of compound **4**: family I (a), family II (b). Backbone is evidenced as a ribbon. Side chains of the 10 lowest energy conformers are also shown as mesh surface. Surfaces are distinguished with different colors. N-Term, N-terminus; C-Term, C-terminus.

have rationally designed and analyzed a limited set of peptides (Table 1). In these peptides, the labile disulfide bridge was replaced by a dicarba-bridge, through the RCM reaction. As can be seen from Table 2, variation of the residues 7 and 10 results in analogues having a low submicromolar potency and a range of sst receptor subtype selectivities.

Recently, we have investigated some octreotide analogues, including compound **3**, in a water/DMSO-d_6 8:2 solution.[13] Here, an NMR study was performed on the developed analogues of octreotide in SDS micelles solution. The use of SDS micelles to study the conformational properties of somatostatin analogues is motivated on the basis of their interaction with a membrane receptor. For peptides acting as ligands of membrane receptors (such as GPCR), the use of membrane mimetic media is suggested, hypothesizing a membrane-assisted mechanism of interactions between the peptides and their receptors.[22] According to this model, the membrane surface plays a key role in facilitating the transition of the peptide from a random coil conformation adopted in the extracellular environment to a conformation that is recognized by the receptor.[23−25] The increase of the local concentration of the peptide and the reduction of the rotational and translational freedom of the neuropeptide are membrane-mediated events which are determinant steps for the conformational transition of the peptide.[26] Actually, we succeeded in correlating the SDS-bound conformation of urotensin-II (U-II), a peptide hormone strictly correlated to somatostatin, to its biological activity.[27]

Some apparently contradictory NOEs were indicative of the presence of at least two conformations in solution for analogues **4**, **5**, and **8**. To deal with this incongruence, we used a practical approach. Incompatible NOEs were considered separately in different calculation cycles. Hence, two families of conformations were obtained which differed mainly in that C-terminal residues were in 3_{10}-helix (family I) or extended (family II) conformation. Eventually, the experimental restraints were fulfilled over the entire ensemble. It is noteworthy that the NMR data of the cognate molecule octreotide, using a single average conformation, reveal several important inconsistencies, including severe violations of mutually exclusive backbone-to-backbone NOEs.[28]

On the basis of the NMR results, some general conformation−affinity relationships concerning the binding to the sst receptors can be outlined. Similar to most of the bioactive analogues of SRIF reported so far,[29] the structures of the peptidomimetics presented here have a β-turn of type II′ spanning residues D-Trp[8] and Lys[9]. The side chain of D-Trp[8] is in the *trans* conformer, and the side chain of Lys[9] is in the

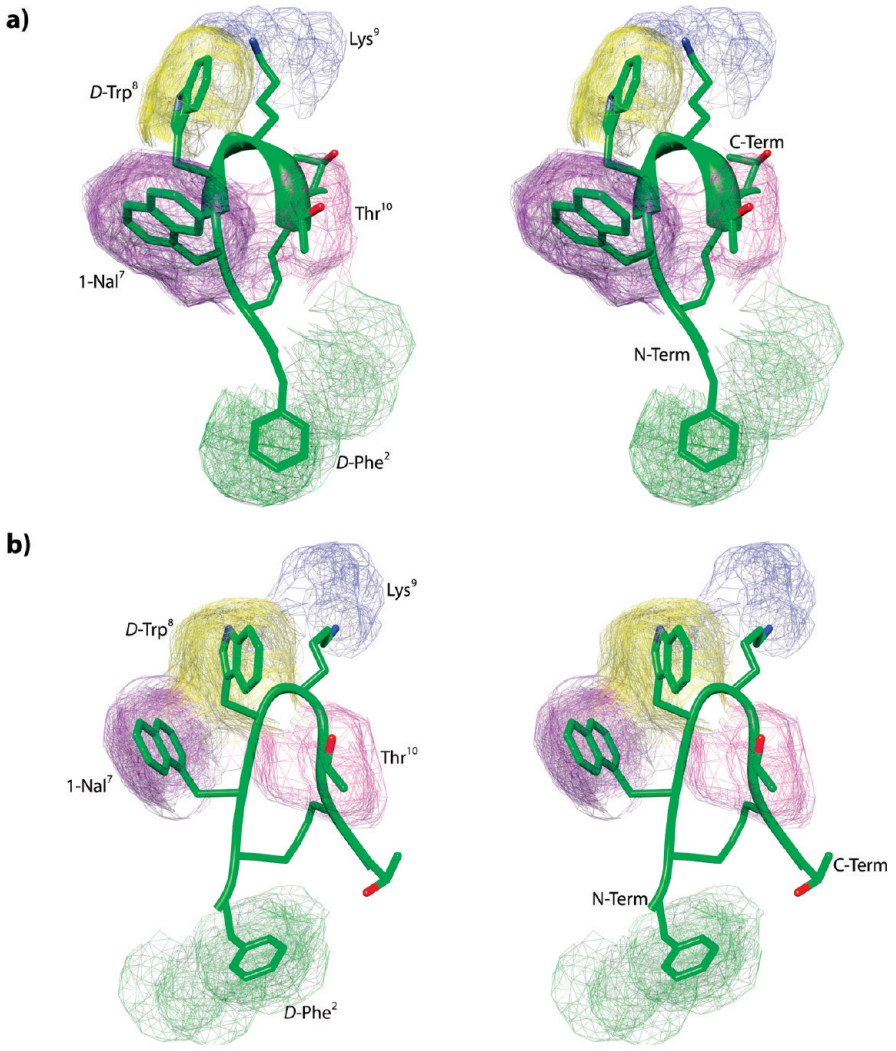

Figure 5. Stereoview of the lowest energy conformer of compound **5**: family I (**a**), family II (**b**). Backbone is evidenced as a ribbon. Side chains of the ten lowest energy conformers are also shown as mesh surface. Surfaces are distinguished with different colors. N-Term, N-terminus; C-Term, C-terminus.

gauche$^-$ conformer, bringing the two side chains adjacent to each other in close proximity. Analogues with the *Z* configuration at the double bond can adopt both helical and extended structures at the C-terminus, showing a conformational equilibrium (Figures 4−6). As a consequence of this conformational behavior, *Z* analogues show greater potency compared to the corresponding *E* isomers (**4** vs **3** and **7** vs **6**) although it can go to the detriment of the selectivity, as in the case of compound **4** compared to **3**. It could be argued, from the data of Table 2, that *Z*-geometry of the double bond is a better mimic of the S−S bridge which, in turn, was hypothesized to be directly involved in the interaction with the sst receptors.[30,31]

Analogues **3** and **4** bear a Tyr(Bzl) residue in position 10. The side chain of Tyr(Bzl)^{10} was designed to replace Phe^6, Phe^7, and Phe^{11} of SRIF14.[32] Compound **3** (*E*-isomer) selectively binds sst_5 while its *Z*-isomer, **4**, showed a pan-SRIF-activity, apart from sst_4. In compound **3**, the β-turn motif is followed by a short 3_{10}-helix along residues Tyr(Bzl)^{10}-dhDsa-C^{14}-Thr(ol)^{15}. The side chain of Tyr(Bzl)^{10} is in the *gauche*$^-$ conformer and is located in close proximity to the D-Trp^8-Lys^9 pair (Figure 3). This is in accordance with our recent results which correlates sst_5 selectivity to conformationally restricted helical structure at the C-terminus.[13] The conformational properties of **3** in SDS micelles are similar to those observed in water/DMSO solution (data not shown). Only N-terminal residue D-Phe^2 is more flexible in the SDS solution compared to DMSO.

In addition to high-affinity binding to $sst_{2,3,5}$ like octreotide (**1**), compound **4** also exhibited a low nanomolar binding to sst_1, hence its affinity pattern resembles that of the hexa-cyclic peptide SOM230 (pasireotide), which also bears a Tyr(bzl)^{10} residue.[32] Because compound **4** fits 4/5 receptor binding sites, it was expected to display a high degree of flexibility. In fact, a dynamical equilibrium between extended and helical conformations was observed. Moreover, Tyr(Bzl)^{10} side chain orientation was different in the two conformations (Figure 4). Notably, NMR[28] and X-ray crystallography analyses have already suggested an equilibrium between extended and folded conformational states for the parent peptide **1**.[33] Furthermore, SOM230 exhibited similar backbone conformational equilibrium in a theoretical MD study; the side chain of Tyr(Bzl) of SOM230 underwent great flexibility which was associated with low selectivity.[34] Although sst_2 is probably the most abundantly expressed SRIF receptor in human cancer,[35] recent literature data indicates that also sst_1 and sst_{3-5} may also be present in some human tumors.[36] Hence, peptides with an improved receptor binding profile are desirable in order to

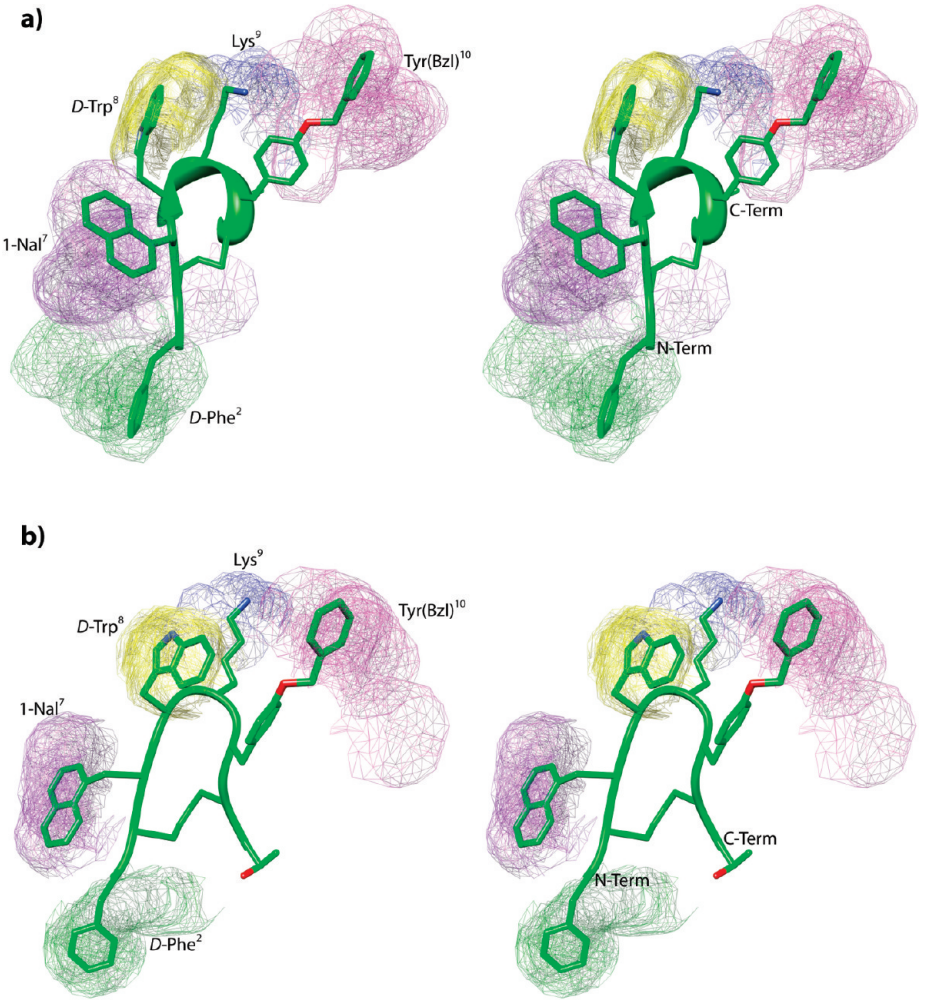

Figure 6. Stereoview of the lowest energy conformer of compound **8**: family I (**a**), family II (**b**). Backbone is evidenced as a ribbon. Side chains of the 10 lowest energy conformers are also shown as mesh surface. Surfaces are distinguished with different colors. N-Term, N-terminus; C-Term, C-terminus.

extend the spectrum of tumors accessible to diagnosis and internal radiotherapy. As a matter of fact, SOM230 is being investigated in clinical trials as a potential treatment for acromegaly, neuroendocrine tumors, and Cushing's disease.[37,38]

Among the tested compounds, peptide **5** showed the highest affinity toward sst_2 and also a good affinity toward sst_5. The sequence of this cyclopeptide is the same as the S−S bridged NOC,[21] whose DOTA derivative, DOTA-NOC, exhibited high affinity toward $sst_{2,3,5}$. The loss of sst_3 affinity in **5** is probably due to the absence of the D-Phe^2-bonded DOTA chelating group. Insertion of different arms at the N-terminus may, in fact, have a dramatic effect, particularly on sst_3 affinity.[39] Compound **5** is also closely related to the previously described compound **2**, sharing its configuration at the double bond and the amino acid sequence but with Nal^7 in replacing Phe^7.[12] The activity profile of analogues **2** and **5** is similar, showing an increase in the sst_2 (∼4-fold) and sst_5 affinity (∼2-fold) of **5** compared to **2** (Table 2). Because **2** showed similar conformational properties as **5** (data not shown), the improved affinity toward sst_2 and sst_5 is probably attributable to the 1-Nal^7 aromatic side chain which, oriented in a *trans* conformation, adequately fits the binding pocket of both receptors.

Compounds **6** and **7** are analogues to **3** and **4**, respectively, with the Tyr(Bzl)^{10} residue replaced by a tyrosine. This change renders compounds **6** and **7** strictly related to U-II. Analogue **6** showed a marked reduction of affinity toward sst_5 compared to the correlated compound **3**. Analogously, compound **7** showed a marked reduction of affinity toward $sst_{1,3,5}$ and a 2-fold reduction toward sst_2 compared to **4**. NMR data of the analogue couples pointed to similar conformational behavior, hence it can be argued that the Tyr^{10} phenol group is detrimental for binding to the sst receptors. This is in accordance with the low affinity of U-II to the sst_{2A} receptor.[40] On the other hand, residual affinity of compound **7** toward sst_2 and sst_5 (Table 2) parallels the capability of U-II to activate these two receptors at high doses.[41]

By combining 1-Nal^7 and Tyr(Bzl)^{10} residue replacements, we obtained compound **8** as a pure *Z*-isomer. Compound **8** showed the highest affinity toward sst_5 (Table 2) with at least a 10-fold selectivity compared to the other ssts. Compound **8** is closely related to compound **4**, sharing its configuration at the double bond and the amino acid sequence but with 1-Nal^7 replacing Phe^7. Actually, the activity profile of the two analogues is similar (pan-SRIF-activity, apart from sst_4) with a decrease of the sst_{1-3} affinity (2- to 4-fold) and increase of the sst_5 activity (∼3-fold) of **8** compared to **4**. The conformational behavior of **8** also resembles that of **4**, in accordance to the activity similarity (Figures 4 and 6). Because the helical-extended conformational equilibrium is also observable in the case of analogue **8**, the affinity changes could be tentatively

Table 3. $C_\gamma - C_\gamma$ Distances (Å) between Putative Pharmacophoric Residues[a]

compd	3	4	5	8	$sst_{2/3/5}$[b]
Ar^2-Ar^7	8.5 ± 0.8[c]	9.0 ± 1.2	9.5 ± 0.5	8.4 ± 1.0	5−11
Ar^2-Ar^8	14.3 ± 0.6	14.0 ± 0.5	14.3 ± 0.6	13.4 ± 0.5	11−15
Ar^2-Lys^9	14.8 ± 0.9	14.4 ± 1.0	13.9 ± 1.0	14.5 ± 1.0	12−15
Ar^2-Ar^{10}	8.1 ± 1.1	7.8 ± 1.2		13.4 ± 1.0	
Ar^7-Ar^8	7.8 ± 0.8	7.6 ± 0.3	6.8 ± 0.2	8.2 ± 0.5	7−9
Ar^7-Lys^9	10.9 ± 0.6	9.8 ± 0.7	9.7 ± 0.3	11.0 ± 0.6	9−11
Ar^8-Lys^9	5.5 ± 0.2	5.6 ± 0.2	4.7 ± 0.3	5.2 ± 0.4	5
Ar^8-Ar^{10}	8.8 ± 0.2	8.9 ± 0.2		8.1 ± 0.1	
Lys^9-Ar^{10}	7.2 ± 0.2	7.2 ± 0.1		5.9 ± 0.2	

[a] Only the family I of peptides **4**, **5**, **8** were considered. [b] Pharmacophore for the sst_2, sst_3, sst_5 selective SRIF analogues.[30] [c] Average distance and standard deviation calculated from the ensemble of 10 structures.

attributed to the orientation of the 1-Nal^7 side chain which was differently oriented in the two peptides. In particular, it passed from a *trans* conformation observed in **4**, to a *gauche*$^-$ conformation in **8**. Such g*auche* orientation of the naphthyl group is likely still suitable (or preferred) for sst_5 but not for sst_{1-3} binding.

On the basis of the results reported above, we updated the previously proposed pharmacophore model for sst_5-selective analogues.[13] The model involves the classical four side chains of the $sst_{2/3/5}$ pharmacophore,[30] namely those of residues D-Phe^2, Phe^7 (Nal^7), D-Trp^8, and Lys^9, plus the $Tyr(Bzl)^{10}$ side chain. The distances between the C_γ atoms of these side chains, observed in the potent sst_5 ligands **3**−**5**, **8** are reported in Table 3. The $C_\gamma - C_\gamma$ distances found by Melacini et al. for the $sst_{2/3/5}$-selective SRIF analogues are also reported in the same table.[30] It can be observed that the distances found in our derivatives agree with the $sst_{2/3/5}$ pharmacophore.

Conclusions

A limited set of compounds of biostable SRIF analogues with dicarba bridge replacing the disulfide bridge of the parent octreotide (**1**) were prepared. Compounds were obtained by on-resin RCM by second generation Grubbs catalyst. All the analogues were tested for their affinity toward the sst_{1-5} receptor subtypes. Among the synthesized compounds, derivative **4** exhibited a pan-somatostatin activity (except sst_4) and derivative **8** exhibited high affinity and selectivity toward sst_5. Actually, compound **8** had a similar sst_5 affinity (IC_{50} 4.9 nM) to SRIF-28 and octreotide. Conformation−affinity relationships confirmed that helical propensity correlates with the peptide sst_5-affinity, while a pan-SRIF activity is obtained by conformational equilibria. Both pan- and selective-SRIF analogues are potentially useful for the diagnosis and internal radiotherapy of tumors.

Experimental Section

General Procedures. Fmoc protected amino acids were purchased from Calbiochem-Novabiochem (Laufelfingen. Switzerland). Second generation Grubbs catalyst was obtained from Aldrich. Fmoc-Hag, Fmoc-*O*-benzyl-L-tyrosine and H-L-Thr(tBu)-ol-2-chlorotrityl resin were purchased from Iris Biotech (Marktredwitz, Germany). HATU was obtained from Chempep (Miami, FL). Peptide grade DMF was from Scharlau (Barcelona, Spain). All the other solvents and reagents used for SPPS were of analytical quality and used without further purification. Analytical RP-HPLCs were performed on a Waters instrument equipped with a UV detector on a Phenomenex Jupiter C18 column (5 μm, 250 mm × 4.6 mm) using a flow rate of 1 mL/min, with the following solvent system: 0.1% TFA in H_2O (A), 0.1% TFA in MeCN (B)). Semipreparative RP-HPLC analyses were performed on the same instrument using a flow rate of 4 mL/min with the same solvent system on a Phenomenex Juppiter C18 column (10 μm, 250 mm × 10 mm). Mass spectra were registered on an ESI LCQ Advantage mass spectrometer (Thermo-Finnigan). LC-ESI-MS analyses were performed on a Phenomenex Jupiter C18 column (5 μm, 150 mm × 2.0 mm) using a flow rate of 500 μL/min on a ThermoFinnigan Surveyor HPLC system coupled to ESI-MS, using the solvent system: H_2O (A), MeCN (B), 1% TFA in H_2O (C). Routine NMR spectra were acquired on a Varian Inova 700 apparatus. TSP was purchased from MSD Isotopes (Montreal, Canada). ^2H_2O was obtained from Aldrich. SDS-d_{25} was obtained from Cambridge Isotope Laboratories, Inc. (Andover, MA). SPPS was performed in Teflon reactor on a manual synthesizer PLS 4 × 4 (AdvancedChemTech). Receptor autoradiography was performed on 20 μm thick cryostat (Microm HM 500, Walldorf, Germany).

Synthesis and Purification of Compounds 3−8. Peptides were synthesized following the method reported in the preceding paper.[13] Briefly, the peptides were prepared using the general Fmoc-SPPS strategy on preswelled H-L-Thr(*t*Bu)-ol-2-chlorotrityl resin. Couplings were performed by adding 2 equiv of protected amino acid activated by HATU and 4 equiv of NMM in DMF. Each coupling was monitored by the qualitative ninhydrin (Kaiser) test.[42] At the end of the linear peptides synthesis, a microscale cleavage was performed. RP-HPLC analysis of the crude products revealed the presence of the linear peptides in approximately 95% purity, without traces of isomers due to amino acid racemization. The cyclization was performed on-resin by second generation Grubbs catalyst (0.5 mol equiv calculated on the basis of 0.5 mmol/g of peptide). After swelling, NH_2 terminal Fmoc−Hag was deprotected and coupled with Fmoc−D-Phe, affording the on-resin peptides **4**−**8**, which were deprotected and cleaved [**5**, **6**, and **7** with TFA/H_2O/EDT/phenol (94:2:2:2, 3 h) while **4** and **8** with TFA/H_2O/EDT/phenol (70:26:2:2, 2.30 h)]. The aqueous solutions of the peptides **4**−**8** were prepurified by SPE and after subjected to the purification by semipreparative RP-HPLC and subsequently characterized by ESI-MS. Analytical RP-HPLC and ESI-MS analysis of the crude compounds revealed two chromatographic peaks with the same MW for compounds **4**−**7**, corresponding to the geometric isomers (Z/E ratio ≈ 90:10). Compounds were then purified by semipreparative RP-HPLC, and the most abundant chromatographic peaks were collected. For all the products, HPLC purity was ≥97%. Further experimental data are reported in the Supporting Information.

NMR Spectroscopy. The samples for NMR spectroscopy were prepared by dissolving the appropriate amount of peptide in 0.55 mL of ^1H_2O (pH 5), 0.05 mL of ^2H_2O to obtain a concentration 1−2 mM of peptides and 200 mM of SDS-d_{25}. TSP was used as internal chemical shift standard. The water signal was suppressed by gradient echo.[43] NMR experiments were recorded on a Varian Inova-Unity 700 MHz at 308.1 K. Complete ^1H NMR chemical shift assignments were effectively achieved for all the analyzed peptides (Tables S3−S8, Supporting Information) according to the Wüthrich procedure[15] via the usual systematic application of TOCSY[16] and NOESY[17] experiments recorded in the phase-sensitive mode using the method from States.[44]

Typical data block sizes were 2048 addresses in t_2 and 512 equidistant t_1 values. Before Fourier transformation, the time domain data matrices were multiplied by shifted $\sin^2$ functions in both dimensions. A mixing time of 70 ms were used for the TOCSY experiments. NOESY experiments were run with mixing times of 100 and 200 ms. The qualitative and quantitative analyses of TOCSY and NOESY spectra were obtained with the support of the XEASY software package.[18]

Structural Determinations and Computational Modeling. The NOE-based distance restraints were obtained from NOESY spectra collected with the mixing time of 100 ms. The NOE cross peaks were integrated with the XEASY program and were converted

into upper distance bounds using the CALIBA program incorporated into the program package DYANA.[19] Only NOE derived constraints (Tables S9−S12, Supporting Information) were considered in the annealing procedures. In a first calculation run, all the upper distance bounds were used, generating an ensemble of 100 structures with the simulated annealing standard protocol of the program DYANA. For peptides **4**, **5**, and **8**, a number of consistent (i.e., in all calculated structures) violated upper limit constraints (>0.1 Å) were observed (Tables S9−S12, Supporting Information). These violations were discarded in a subsequent MD run. This step was repeated until no violation was observed (two runs were enough for all peptides). Thus, we obtained a first family of structures (family I). In a second MD cycle, the violated upper limit constraints of the first cycle were upweighted (10-fold) for the contribution to the target energy function of DYANA. Hence, we obtained a new set of violated constraints which were discarded in the subsequent MD runs. After two MD runs, no violations were observed. In the final calculation run, we applied the same weight to the undiscarded constraints and obtained a second family of structures (family II). Because the two sets of violations had no common member, we did not repeat further the described procedure.

Finally, 20 structures for peptide **3** and 20 structures for each family of peptides **4**, **5**, and **8** were chosen whose interprotonic distances best fitted NOE derived distances and then refined through successive steps of restrained and unrestrained energy minimization calculations using the Discover algorithm (Accelrys, San Diego, CA) and the consistent valence force field (CVFF).[45]

The minimization lowered the total energy of the structures. The final structures were analyzed using the InsightII program (Accelrys, San Diego, CA). Graphical representation were carried out with the UCSF Chimera package.[46] The root-mean-squared-deviation analysis between energy-minimized structures were carried out with the program MOLMOL.[47]

Determination of Somatostatin Receptor Affinity Profiles. Cell membrane pellets were prepared from human sst_1-expressing CHO cells, sst_2-, sst_3-, sst_4-expressing CCL39 cells, and sst_5-expressing HEK293 cells and stored at −80 °C. Receptor autoradiography was performed on 20 μm thick cryostat (Microm HM 500, Walldorf, Germany) sections of the membrane pellets, mounted on microscope slides, and then stored at −20 °C as previously described.[48,49] For each of the tested compounds, complete displacement experiments with the universal SRIF radioligand [Leu^8, D-Trp^{22}, ^{125}I-Tyr^{25}]-SRIF-28 (^{125}I-[LTT]-SRIF-28) (2000 Ci/mmol; Anawa, Wangen, Switzerland) using 15000 cpm/100 μL and increasing concentrations of the unlabeled peptide ranging from 0.1 to 1000 nM were performed. As control, unlabeled SRIF-28 was run in parallel using the same increasing concentrations. The sections were incubated with ^{125}I-[LTT]-SRIF-28 for 2 h at room temperature in 170 mmol/L Tris-HCl buffer (pH 8.2), containing 1% BSA, 40 mg/L bacitracin, and 10 mmol/L $MgCl_2$ to inhibit endogenous proteases. The incubated sections were washed twice for 5 min in cold 170 mmol/L Tris-HCl (pH 8.2) containing 0.25% BSA. After a brief dip in 170 mmol/L Tris-HCl (pH 8.2), the sections were dried quickly and exposed for 1 week to Kodak BioMax MR film. IC_{50} values were calculated after quantification of the data using a computer-assisted image processing system as described previously.[49] Tissue standards (Autoradiographic [^{125}I] and/or [^{14}C] microscales, GE Healthcare; Little Chalfont, UK) that contain known amounts of isotope, cross-calibrated to tissue-equivalent ligand concentrations, were used for quantification.[3]

Acknowledgment. The NMR spectral data were provided by Centro di Ricerca Interdipartimentale di Analisi Strumentale, Università degli Studi di Napoli "Federico II". The assistance of the staff is gratefully appreciated. We also acknowledge the Advanced Accelerator Applications Spa and the Ente Cassa di Risparmio of Florence for funding and for providing a scholarship.

Supporting Information Available: Analytical data of the synthesized peptides and NMR data of the analyzed peptides. Atomic coordinates of the lowest energy conformer of compounds **3**, **4**, **5**, and **8**. This material is available free of charge via the Internet at http://pubs.acs.org.

References

(1) Burgus, R.; Brazeau, P.; Vale, W. W. Isolation and determination of the primary structure of somatostatin (a somatotropin release inhibiting factor) of bovin hypothalamic origin. *Advances in Human Growth Hormone Research, Report no. 74-612*; U.S. Government Printing Office, DHEW, (NIH): Washington, DC, **1973**; pp 144−158.

(2) Weckbecker, G.; Lewis, I.; Albert, R.; Schmid, H. A.; Hoyer, D.; Bruns, C. Opportunities in somatostatin research: biological, chemical and therapeutical aspects. *Nature Rev. Drug Discovery* **2003**, *2*, 999–1018.

(3) Erchegyi, J.; Cescato, R.; Grace, C. R.; Waser, B.; Piccand, V.; Hoyer, D.; Riek, R.; Rivier, J. E.; Reubi, J. C. Novel, and radioiodinable somatostatin receptor 1 (sst_1) selective analogues. *J. Med. Chem.* **2009**, *52*, 2733–2764and references therein. .

(4) Grace, C. R. R.; Erchegyi, J.; Koerber, S. C.; Reubi, J. C.; Rivier, J. E.; Riek, R. Novel sst2-selective somatostatin agonists. Three-dimensional consensus structure by NMR. *J. Med. Chem.* **2006**, *49*, 4487–4496.

(5) Gairì, M.; Saiz, P.; Madurga, S.; Roig, X.; Erchegyi, J.; Koerber, S. C.; Reubi, J. C.; Rivier, J. E.; Giralt, E. Conformational analysis of a potent SSTR3-selective somatostatin analogue by NMR in water solution. *J. Pept. Sci.* **2006**, *12*, 82–91.

(6) Grace, C. R.; Koerber, S. C.; Erchegyi, J.; Reubi, J. C.; Rivier, J.; Riek, R. Novel sst(4)-selective somatostatin (SRIF) agonists. 4. Three-dimensional consensus structure by NMR. *J. Med. Chem.* **2003**, *46*, 5606–5618.

(7) Bauer, W.; Briner, U.; Dopfener, W.; Haller, R.; Huguenin, R.; Marbach, P.; Petcher, T. J.; Pless, J. SMS 201-995: a very potent and selective analogue of somatostatin with prolonged action. *Life Sci.* **1982**, *31*, 1133–1140.

(8) Ginj, M.; Schmitt, J. S.; Chen, J.; Waser, B.; Reubi, J. C.; de Jong, M.; Schulz, S.; Mäcke, H. R. Design, synthesis, and biological evaluation of somatostatin-based radiopeptides. *Chem. Biol.* **2006**, *13*, 1081–1090.

(9) Ginj, M.; Zhang, H.; Waser, B.; Cescato, R.; Wild, D.; Wang, X.; Erchegyi, J.; Rivier, J.; Mäcke, H.; R. Reubi, J. C. Radiolabeled somatostatin receptor antagonists are preferable to agonists for in vivo peptide receptor targeting of tumors. *Proc. Natl. Acad. Sci. U.S.A.* **2006**, *103*, 16436–16441.

(10) de Jong, M.; Breeman, W. A. P.; Kwekkenboom, D. J.; Valkema, R; Krenning, E. P. Tumor imaging and therapy using radiolabeled somatostatin analogues. *Acc. Chem. Res.* **2009**, *42*, 873–880and references therein. .

(11) Fichna, J.; Janecka, A. Synthesis of target-specific radiolabeled peptides for diagnostic imaging. *Bioconjugate Chem.* **2003**, *14*, 3–17.

(12) Carotenuto, A.; D'Addona, D.; Rivalta, E.; Chelli, M.; Papini, A. M.; Rovero, P.; Ginanneschi, M. Synthesis of a dicarba-analogue of octreotide keeping the type II′ β-turn of the farmacophore in water solution. *Lett. Org. Chem.* **2005**, *2*, 274–279.

(13) D'Addona, D.; Carotenuto, A.; Novellino, E.; Piccand, V.; Reubi, J. C.; Di Cianni, A; Gori, F.; Papini, A. M.; Ginanneschi, M. Novel sst5-selective somatostatin dicarba anlogues: synthesis and conformation−affinity relationships. *J. Med. Chem.* **2008**, *51*, 512–520.

(14) Barragán, F.; Moreno, V.; Marchan, V. Solid-phase synthesis and DNA binding studies of dichloroplatinum(II) conjugates of dicarba analogues of octreotide as new anticancer drugs. *Chem. Commun.* **2009**, 4705–4707.

(15) Wütrich, K. *NMR of Proteins and Nucleic Acids*; John Wiley & Sons, Inc: New York, 1986.

(16) Braunschweiler, L.; Ernst, R. R. Coherence Transfer by isotropic mixing: application to proton correlation spectroscopy. *J. Magn. Reson.* **1983**, *53*, 521–528.

(17) Jenner, J.; Meyer, B. H.; Bachman, P.; Ernst, R. R. Investigation of exchange processes by two-dimensional NMR spectroscopy. *J. Chem. Phys.* **1979**, *71*, 4546–4553.

(18) Bartels, C.; Xia, T.; Billeter, M.; Güntert, P.; Wüthrich, K. The program XEASY for computer-supported NMR spectral analysis of biological macromolecules. *J. Biomol. NMR* **1995**, *6*, 1–10.

(19) Güntert, P.; Mumenthaler, C.; Wütrich, K. Torsion angle dynamics for NMR structure calculation with the new program DYANA. *J. Mol. Biol.* **1997**, *273*, 283–298.

(20) Arison, B. H.; Hirschmann, R.; Veber, D. F. Inferences about the conformation of somatostatin at a biologic receptor based on NMR studies. *Bioorg. Chem.* **1978**, *7*, 447–451.
(21) Wild, D.; Schmitt, J. S.; Ginj, M.; Mäcke, H. R.; Bernard, B. F.; Krenning, E.; de Jong, M.; Wenger, S.; Reubi, J. C. DOTA-NOC, a high-affinity ligand of somatostatin receptor subtypes 2, 3 and 5 for labelling with various radiometals. *Eur. J. Med. Mol. Imaging* **2003**, *30*, 1338–1347.
(22) Moroder, L.; Romano, R.; Guba, W.; Mierke, D. F.; Kessler, H.; Delporte, C.; Winand, J.; Christophe, J. New evidence for a membrane bound pathway in hormone receptor binding. *Biochemistry* **1993**, *32*, 13551–13559.
(23) Wienk, H. L.; Wechselberger, R. W.; Czisch, M.; de Kruijff, B. Structure, dynamics, and insertion of a chloroplast targeting peptide in mixed micelles. *Biochemistry* **2000**, *39*, 8219–8227.
(24) Bryson, E. A.; Rankin, S. E.; Carey, M.; Watts, A.; Pinheiro, T. J. Folding of apocytochrome c in lipid micelles: formation of α helix precedes membrane insertion. *Biochemistry* **1999**, *38*, 9758–9767.
(25) Yamamoto, T.; Nair, P.; Jacobsen, N. E.; Davis, P.; Ma, S. W.; Navratilova, E.; Moye, S.; Lai, J.; Yamamura, H. I.; Vanderah, T. W.; Porreca, F.; Hruby, V. J. The importance of micelle-bound states for the bioactivities of bifunctional peptide derivatives for δ/μ opioid receptor agonists and neurokinin 1 receptor antagonists. *J. Med. Chem.* **2008**, *51*, 6334–6347.
(26) Sargent, D. F.; Schwyzer, R. Membrane lipid phase as catalyst for peptide−receptor interactions. *Proc. Natl. Acad. Sci. U.S.A.* **1986**, *83*, 5774–5778.
(27) Grieco, P.; Carotenuto, A.; Campiglia, P.; Gomez-Monterrey, I.; Auriemma, L.; Sala, M.; Marcozzi, C.; d'Emmanuele di Villa Bianca, R.; Brancaccio, D.; Rovero, P.; Santicioli, P.; Meini, S.; Maggi, C. A.; Novellino, E. New insight into the binding mode of peptide ligands at Urotensin-II receptor: structure−activity relationships study on P5U and Urantide. *J. Med. Chem.* **2009**, *52*, 3927–3940.
(28) Melacini, G.; Zhu, Q.; Goodman, M. Multiconformational NMR analysis of sandostatin (octreotide): equilibrium between beta-sheet and partially helical structures. *Biochemistry* **1997**, *36*, 1233–1241.
(29) Tyndall, J. D. A.; Pfeiffer, B.; Abbenante, G.; Fairlie, D. P. Over one hundred peptide-activated G protein-coupled receptors recognize ligands with turn structure. *Chem. Rev.* **2005**, *105*, 793–826.
(30) Melacini, G.; Zhu, Q.; Osapay, G.; Goodman, M. A. Refined model for the somatostatin pharmacophore: conformational analysis of lanthionine−sandostatin analogs. *J. Med. Chem.* **1997**, *40*, 2252–2258.
(31) Brady, S. F.; Paleveda, W. J.; Arison, B. H.; Saperstein, R.; Brady, E. J.; Raynor, K.; Reisine, T.; Veber, D. F.; Freidinger, R. M. Approaches to peptidomimetics which serve as surrogates for the *cis* amide bond: novel disulfide-constrained bicyclic hexapeptide analogs of somatostatin. *Tetrahedron* **1993**, *49*, 3449–3466.
(32) Lewis, I.; Bauer, W.; Albert, R.; Chandramouli, N.; Pless, J.; Weckbecker, G.; Bruns, C. A novel somatostatin mimic with broad somatotropine release inhibitory factor receptor binding and superior therapeutic potential. *J. Med. Chem.* **2003**, *46*, 2334–2344.
(33) Pohl, E.; Heine, A.; Sheldrick, G. M.; Dauter, Z.; Wilson, K. S.; Kallen, J.; Huber, W.; Pfaffli, P. J. Structure of octreotide, a somatostatin analog. *Acta Crystallogr., Sect. D: Biol. Crystallogr.* **1995**, *51*, 48–59.
(34) Interlandi, G. Backbone conformations and side chain flexibility of two somatostatin mimics investigated by molecular dynamics simulations. *Proteins* **2009**, *75*, 659–670.
(35) Reubi, J. C.; Waser, B.; Schaer, J.; Laissue, J. A. Somatostatin receptor sst1−sst5 expression in normal and neoplastic human tissues using receptor autoradiography with subtype-selective ligands. *Eur. J. Nucl. Med.* **2001**, *28*, 836–846.
(36) Zatelli, M. C.; degli Umberti, E. The significance of new somatostatin analogs as therapeutic agents. *Curr. Opin. Invest. Drugs* **2009**, *10*, 1025–1031.
(37) Ben-Shlomo, A.; Melmed, S. Pasireotide-A somatostatin analog for the potential treatment of acromegaly, neuroendocrine tumors and Cushing's disease. *IDrugs* **2007**, *10*, 885–895.
(38) Cescato, R.; Loesch, K. A.; Waser, B.; Mäcke, H. R.; Rivier, J. E.; Reubi, J. C.; Schonbrunn, A. Agonist-biased signaling at the sst2A receptor: the multi-somatostatin analogs KE108 and SOM230 activate and antagonize distinct signaling pathways. *Mol. Endocrinol.* **2010**, *24*, 240–249.
(39) Antunes, P.; Ginj, M.; Walter, M. A.; Chen, J.; Reubi, J. C.; Mäcke, H. R. Influence of different spacers on the biological profile of a DOTA-somatostatin analogue. *Bioconjugate Chem.* **2007**, *18*, 84–92.
(40) Nothacker, H. P.; Wang, Z.; McNeill, A. M.; Saito, Y.; Merten, S.; O'Dowd, B.; Duckles, S. P.; Civelli, O. Identification of the natural ligand of an orphan G-protein-coupled receptor involved in the regulation of vasoconstriction. *Nature Cell Biol.* **1999**, *1*, 383–385.
(41) Malagon, M. M.; Molina, M.; Gahete, M. D.; Duran-Prado, M.; Martinez-Fuentes, A. J.; Alcain, F. J.; Tonon, M. C.; Leprince, J.; Vaudry, H.; Castaño, J. P.; Vazquez-Martinez, R. Urotensin II and urotensin II-related peptide activate somatostatin receptor subtypes 2 and 5. *Peptides* **2008**, *29*, 711–720.
(42) Stewart, J. M.; Young, J. D. In *Solid Phase Peptide Synthesis*, 2nd ed.; Pierce Chemical Company: Rockford, IL, 1984.
(43) Hwang, T. L.; Shaka, A. J. Water suppression that works. Excitation sculpting using arbitrary wave-forms and pulsed-field gradients. *J. Magn. Reson.* **1995**, *112*, 275–279.
(44) States, D. J.; Haberkorn, R. A.; Ruben, D. J. A two-dimensional nuclear Overhauser experiment with pure absorption phase four quadrants. *J. Magn. Reson.* **1982**, *48*, 286–292.
(45) Maple, J.; Dinur, U.; Hagler, A. T. Derivation of force field for molecular mechanics and dynamics from ab initio energy surface. *Proc. Natl. Acad. Sci. U.S.A.* **1988**, *85*, 5350–5354.
(46) Pettersen, E. F.; Goddard, T. D.; Huang, C. C.; Couch, G. S.; Greenblatt, D. M.; Meng, E. C.; Ferrin, T. E. UCSF Chimera—a visualization system for exploratory research and analysis. *J. Comput. Chem.* **2004**, *25*, 1605–1612.
(47) Koradi, R.; Billeter, M.; Wüthrich, K. MOLMOL: a program for display and analysis of macromolecular structures. *J. Mol. Graphics* **1996**, *14*, 51–55.
(48) Reubi, J. C.; Schaer, J. C.; Waser, B.; Wenger, S.; Heppeler, A.; Schmitt, J. S.; Mäcke, H. R. Affinity profiles for human somatostatin receptor sst_1−sst_5 of somatostatin radiotracers selected for scintigraphic and radiotherapeutic use. *Eur. J. Nucl. Med.* **2000**, *27*, 273–282.
(49) Cescato, R.; Erchegyi, J.; Waser, B.; Piccand, V.; Mäcke, H. R.; Rivier, J. E.; Reubi, J. C. Design and in vitro characterization of highly sst_2-selective somatostatin antagonists suitable for radiotargeting. *J. Med. Chem.* **2008**, *51*, 4030–4037.